10.1515/tvsb-2015-0020

Transactions of the VŠB – Technical University of Ostrava

Civil Engineering Series, No. 2, Vol. 15, 2015

paper #20

Tomasz PONIKIEWSKI[1], Jacek GOŁASZEWSKI[2]

X-RAY INVESTIGATION AND MODELLING OF STEEL FIBRES IN SELF-COMPACTING CONCRETE

Abstract

The paper presents an analysis of cross-sections of beams made of Steel Fiber Reinforced High Performance Self-Compacting Concrete (SFRHPSCC). The analysis was performed by two methods, using our own computer program (destructive method), and computed tomography (non-destructive method). Statistical analysis showed that the orientation of the fibers exhibit exponential distribution. The tests confirmed the correct formation of concrete, maintaining the uniformity of steel fibre distribution.

Keywords

Steel fibre, high-performance self-compacting concrete, fibre orientation, rheology, workability, Bingham model, X-ray Computed Tomography.

1 INTRODUCTION

The effect of steel fibres content on the self-compatibility of concrete mixture as well as on the mechanical properties of hardened concrete has already been investigated. Previous studies on SFRHPSCC have not provided systematic, validated experimental data to enable their design for their assumed mechanical parameters as well as the distribution and orientation of the dispersed reinforcement [1, 2, 3]. This causes the discrepancy between the projected and obtained mechanical parameters of the modified concretes [4, 5]. It is important to determine the degree of variation of the assumed mechanical properties of SFRHPSCC due to the location and orientation of the dispersed reinforcement [6, 7]. These research results should form the basis for development of the design method for SFRHPSCC applied to selected molded components.

The presented research is a basis for identifying the behavior of fibres with different geometrical parameters in the matrix of self-compacting concrete, taking into account the assumed differentiated states of stress. In view of the diversity of the currently used steel fibres and high impact the formation methods have on the homogeneity of the mixture, forming SFRHPSCC of the assumed mechanical properties is difficult, which creates the desire for additional research [8,9,14,15,16]. Results of previous studies of self-compacting fiber concrete indicate that their self-thickening and physical-mechanical properties are mainly determined by the geometric parameters of fibres and their volume ratio in concrete mix. However, in previous publications, there has been no assessment of the impact on methods of forming SFRHPSCC have on their physical-mechanical properties, which in the case of these concretes is a substantial problem. Currently, fibre reinforcement is treated as an additive to concrete which improves its properties, but not as structural reinforcement (there are already examples of completed construction). In this approach, a uniform distribution of reinforcement can be considered safe, but not optimal [10,11,13]. In the future we

[1] Tomasz Ponikiewski, Silesian University of Technology, Akademicka 5, 44-100 Gliwice, Poland, Tomasz.Ponikiewski@polsl.pl.

[2] Jacek Gołaszewski, Silesian University of Technology, Akademicka 5, 44-100 Gliwice, Poland, Jacek.Golaszewski@polsl.pl.

expect development of concrete structures reinforced only by fibres. The formation effect on the orientation and uniformity of distribution of fibres must be considered in designing of such structures. This study provides the first systematic data that can be used for this purpose.

2 RESEARCH SIGNIFICANCE

The main aim of this study was to determine the distribution and orientation of reinforcement in SFRHPSCC. This will allow the design of concrete structures with anticipated deployment of the dispersed reinforcement, specific to the structural elements and method of its formation. The core of the problem is to determine how in various structures the deployment of the dispersed reinforcement is dependent on the laying of the mixture, taking into account its rheological properties, the volume ratio and geometric parameters of the steel fibres. The research results can be used to improve the accuracy of modeling the mechanical properties of selected elements of structures with dispersed reinforcement. This will allow better optimization of the use of fibres in a matrix of concrete, which in some cases is a good alternative to traditional reinforcement, identifying and reducing the technological limitations. This research project results may be the starting point for further, more advanced research, including complex concrete structural elements, or leading to proposals for fibre directionality factors to be applied in procedures and standards.

3 EXPERIMENTAL PROCEDURE

3.1 Rheological properties of cement binder's mixture and their measurement

Laboratory studies have shown and it has commonly accepted that rheological behavior of concrete may be sufficiently described by the Bingham model according to equation:

$$\tau = \tau_o + \eta_{pl} \bullet \dot{\gamma} \quad (1)$$

where: τ (Pa) is the shear stress at shear rate γ (1/s) and τ_o (Pa) and η_{pl} (Pas) are the yield stress and plastic viscosity, respectively. Yield stress determines the value of shear stress necessary for initiating flow. When the shear stress (τ) surpasses the yield stress, the flow of the mixture occurs and the resistance of the flow depends on plastic viscosity; the bigger the plastic viscosity of the mixture, the slower it can flow.

Rheological parameters of fresh concrete, can be measured using Two Point Workability Test (TPWT), by applying a given shear rate and measuring the resulting shear stress [12]. In the TPWT the rheological parameters of fresh concrete are measured by applying a given shear rate and measuring the resulting shear stress (Fig. 1).

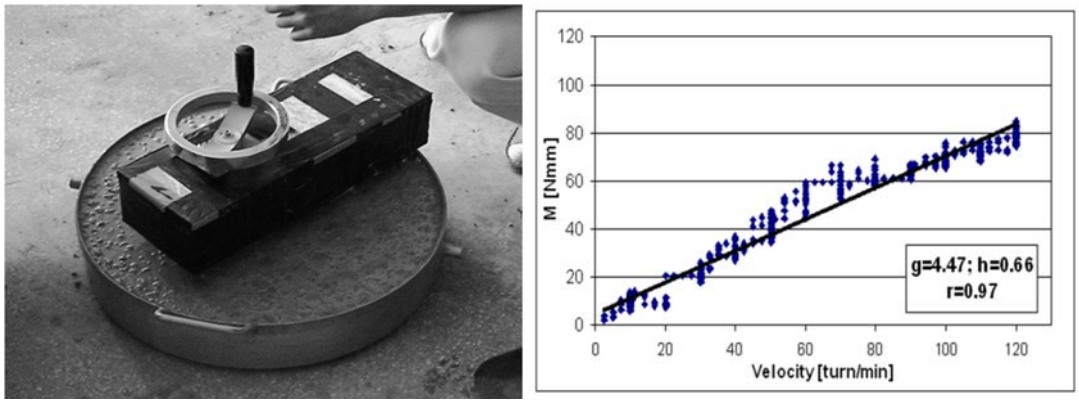

Fig. 1: BT-2 concrete rheometer and procedure to determine *g* and *h* values

The rheological parameters are determined by regression analysis according to the relation:

$$T = g + N\,h \qquad (2)$$

where: T is the shear resistance of a sample measured at rotation rate N and g (Nmm) and h (Nmms) are constants corresponding respectively to yield value τ_o and plastic viscosity η_{pl}. By suitable calibration of the rheometer, it is possible to express g and h in fundamental units.

3.2 Specimens

The uniformity of distribution of steel fibers has been studied in SFRHPSCC formed into beams with dimensions of 600x150x150 mm (Fig. 2).

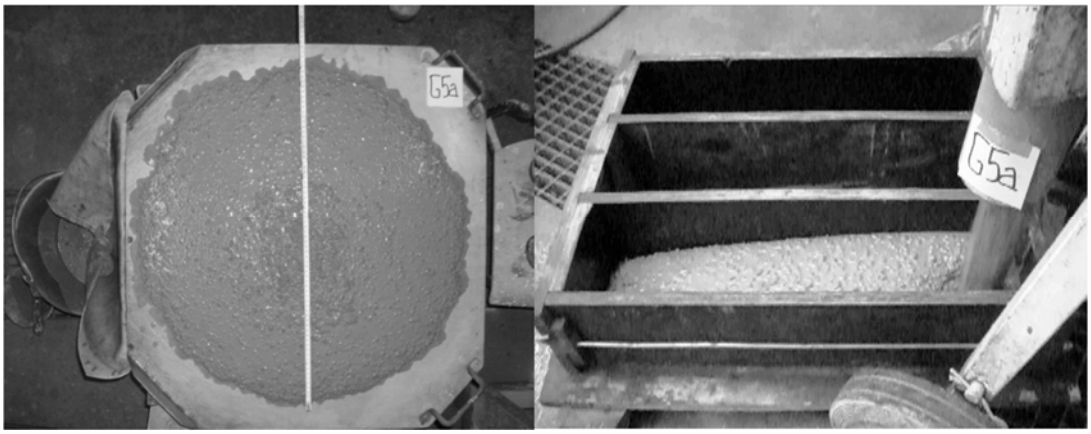

Fig. 2: Slump-flow test and forming SFRHPSCC beam C4 600x150x150 mm

Tests of concretes were made by digital image analysis (destructive method - Fig. 3) and computed tomography (non-destructive method - Fig. 4).

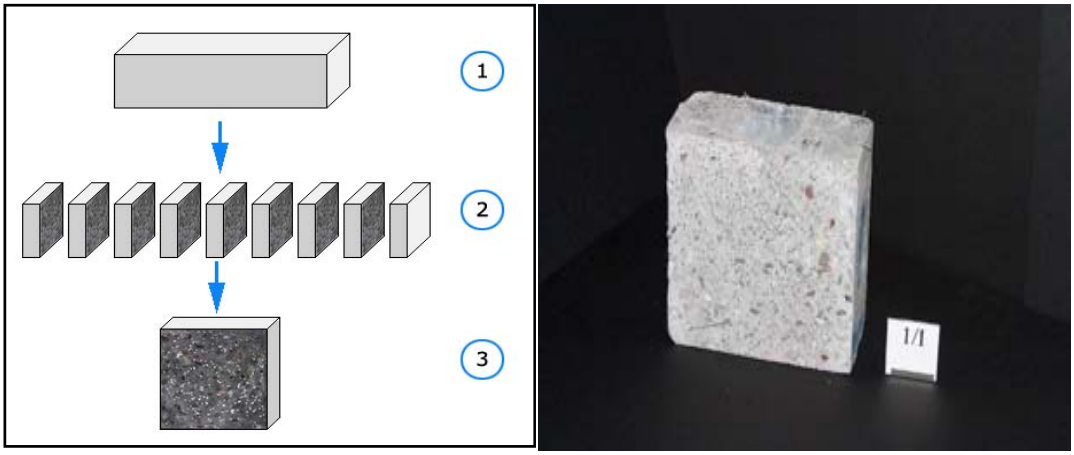

Fig. 3: Phases of micro-section preparation and a specimen prepared for analysis

Fig. 4: The CT scanner applied for this research was equipped with 64 rows of detectors, and the thickness of a series of reconstructed native CT scan was 0.625 mm

In order to smooth the image analysis of concrete with distributed steel fibres, we developed a program whose mission is to find the cut fibers and to describe their position in the sample. This developed program was used to evaluate the homogeneity of distribution of steel fibers in self-thickening concrete.

The paper also presents the results of the computer tomography. The CT scanner applied for this research was equipped with 64 rows of detectors, and the thickness of a series of reconstructed native CT scan was 0.625 mm, i.e. the width of a single detector. The penetration factor in the study was an X-ray beam. The dimension of the surface of each layer of concrete was 150x150 mm. For each beam the result consisted of a native series written in DICOM format with at least 950 images, and reconstructed series with at least 1500 images taking into account the interval in the range 50 ÷ 80% of the thickness of the native layer. Parameters of acquisition were not less than: 140kvP lamp voltage, 400 mAs.

3.3 Materials

The composition of the investigated compounds of HPSCC is shown in Table 1.

Tab. 1: Composition of SFRHPSCC mixture kg/m^3

Component	**Symbol**	**Content**
CEM I 42,5 R	*C*	490
Sand 0–2 mm	*S*	756
Basalt 2–8 mm	*B*	944.4
Silica fume	*SF*	49
Water	*W*	226.4
Steel fibres – kg/m^3 (% by volume)	*F*	100 – 180 (1.25 – 2.25)
Superplasicizer Glenium ACE 48 (3.5 % m.c.)	*SP*	17
Stabilizer RheoMatrix (0.4 % m.c.)	*ST*	1.6
W/(C+SF)	-	0.42
Slump-flow (SF)	-	SF3

They were considered in the study two types of steel fibres (Table 2) for different volume ratios (Table 3).

Tab. 2: Characteristics of steel fibres using in research

Name	Length	Diameter	Cross-section	Shape	Tensile strength (N/mm^2)
	(mm)	(mm)			
KE 20/1.7	20±10%	1.70±10%	rectangular [1)]		770±15%
SW 35/1.0	35±10%	2.30±2.95 [2)]	part of circle		800±15%

Designations: [1)] thickness 0.50±10%; [2)] width (mm);

Tab. 3: The characteristics of steel fibres and their percentage in the mixture

Mixture	Content of fibres, % by volume	
	KE 20/1,7	SW 35/1.0
C0	-	-
C1	1.25	-
C2	2.25	-
C3	-	1.25
C4	-	2.25

The self-compacting criterion was met by all tested concretes, according to prepared mixing procedure (Fig. 5).

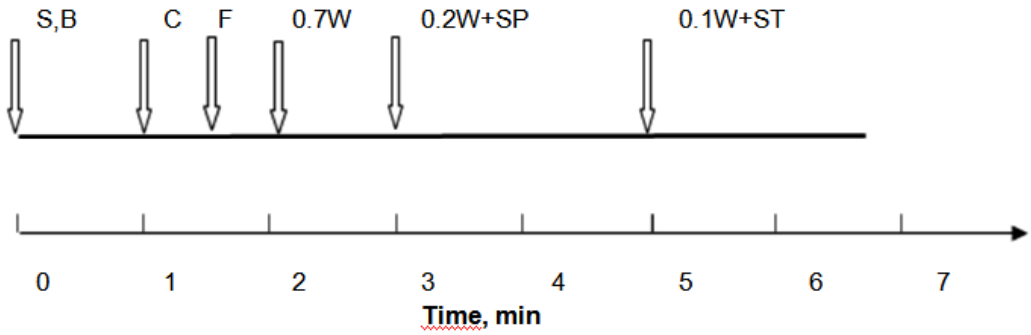

Fig. 5: Mixing procedure for SFRHPSCC

The detailed results are presented for compounds with the fiber content 1.25 and 2.25% (90 and 180 kg/m3). In Table 4 the results for investigated SFRHPSCC mixtures are presented. The ability of self compaction was verified by measurements of time and flow diameter using the Abrams cone as well as basing on the values of rheological parameters by rheological procedure. The compressive strength was measured after the 28 day storage. For effective analysis of scattered fibres reinforced concrete the computer program has been used; the accuracy of results depends only upon the resolution of analyzed image. The program finds the intersections of fibres on the surface and their orientation. Some steps can be distinguished when the program operates. At first, the area of analyzed part of the image is delineated. In this stage the virtual table of colors is created in which the contents of particular meshes correspond with the colors.

Tab. 4: The properties of fresh and hardened SFRHPSCC mixtures

Mixture	Workability				$f_{c,cube\ 28}$ [MPa]
	Slump-flow		Rheological parameters		
	T_{500} [s]	SF [mm]	g [Nmm]	h [Nmmmin]	
C0	3	750	88	1 457	90
C1	4	700	105	3 008	105
C2	5	650	362	3 146	110
C3	2	740	160	2 802	95
C4	3	690	421	1 596	100

The next step of image recognition consists in elimination of those meshes which represent the values under the assumed limit. After this operation the table of colors transforms into the logic table which contains only the values 0 or 1; it means that in the mesh there is a part of analyzed fibers or there is no fibers. Because the transfer from the real color scale to the grey color scale leads always to the loss of some information, the next step consists in filling and rounding the contours of fibers. The new table, determining the number of fibres and some other data is formed. In the next step the program eliminates too small or too large areas which could be positively identified as fibre cross sections. Finally the results of image analysis are highlighted. The values determining the amount of fibres present in every square area are generated.

4 METHODS

Image processing was implemented using open-source medical image processing C++ libraries The Insight Toolkit (ITK) [17]. Statistical data analysis was performed using STATISTICA and MATLAB software.

4.1 Image Processing

Let I_0 denote the acquired volumetric CT intensity image [18, 19]. First stage of the image processing was responsible for automatic determination of the volume of interest (VOI) in order to perform subsequent analyses only on the concrete beam and consists of the following:

1. initial binarization above 500 Hounsfield Units (HU),
2. binary image labeling,
3. selection of the largest object,
4. VOI coordinates retrieval from the smallest rectangular cuboid circumscribed over the object selected in step 3.

Further processing was performed only within the VOI (done by image cropping, Fig. 1(a)) and consisted of the following steps:

1. image framing I_0 to beam area
2. binarization of the image I_0 above 3000HU,
3. binary median filtering,
4. separation of objects similar to [11],
5. binary image labeling with rejection of objects smaller than 100 [mm^3] and larger than 300 [mm^3],
6. for each object within the label image its geometrical center and orientation was found. Orientation was defined with the eigenvector corresponding to the smallest eigenvalue of the object's rotation matrix.

Fibers segmentation results are shown in Figure 6(b).

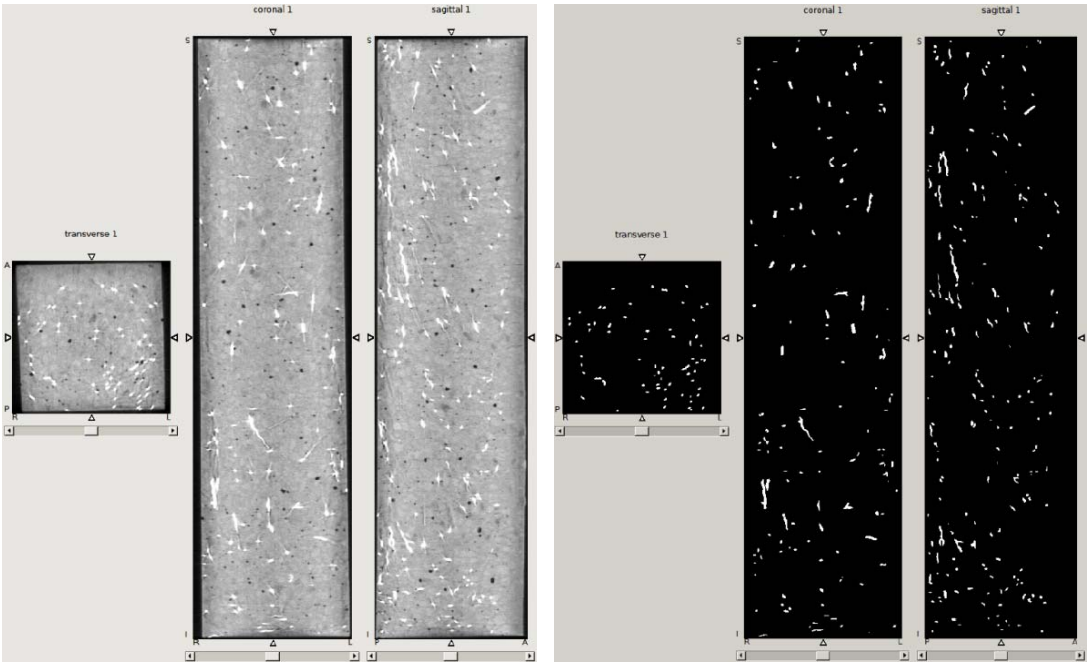

Fig. 6: Cross sections of an exemplary beam: (a) image after VOI selection, (b) after steel fibers segmentation

4.2 Statistical Analysis

For each fiber in the analyzed beam the data retrieved during the image analysis was as follows [18]:

- label defining each fiber,
- coordinates of the fiber center in 3D,
- eigenvector of the fibers's rotation matrix corresponding to the smallest eigenvalue,
- volume of the fiber.

Having the above mentioned values, spherical histograms can be generated following the presented steps. The total number of fibers is labeled with *n*.

1. For each fiber obtained vector υ_k is parallel to its main axis
$$\forall k \in \{1,2,\dots,n\} \quad \upsilon_k = (\upsilon_{k,1}, \upsilon_{k,2}, \upsilon_{k,3}) \tag{2}$$
2. For each fiber vector υ_k assigned to the fiber, should be provided using spherical coordinates
$$\forall k \in \{1,2,\dots,n\} \quad \upsilon_k = (\varphi_k, \theta_k, r_k) \tag{3}$$
3. For each vector parallel to a fiber φ_k a new vector ω_k is assigned, whose two first coordinates are angles φ_k, θ_k and its third coordinate equals 1
$$\forall k \in \{1,2,\dots,n\} \quad \omega_k = (\omega_{k,1}, \omega_{k,2}, \omega_{k,3}) = (\varphi_k, \theta_k, 1) \tag{4}$$
4. Let c be the number of groups to which each angle parameter is divided. The value of c should be a divisor of 180
$$(c \in \{1,2,3,4,5,6,9,10,12,15,18,20,30,36,45,60,90,180\})$$

and it is set for both φ and θ. This gives a total number of c^2 groups of equal width intervals for these angles.

5. Let ni,j be the number of vectors ωi that belong to the i-th group in terms of angle φ and in the *j*-th group in terms of angle θ_0
$$\forall i \in \{1,2,\dots,c\}, \forall j \in \{1,2,\dots,c\}, n_{i,j} = \sum_{k=1}^{n} \chi\, S_{i,j}(\omega_k), \tag{5}$$
where χ is the characteristic function defined as
$$\chi S_{i,j}(\omega_k) = \begin{cases} 1, \omega_k \in S_{i,j} \\ 0, \omega_k \notin S_{i,j} \end{cases}$$
where the set $S_{i,j}$ is defined as follows
$$\forall i \in \{1,2,\dots,c\}, \forall j \in \{1,2,\dots,c\}$$
$$S_{i,j} = \left\{(\varphi,\theta): \quad \frac{180}{c}\cdot(i-1) \le \varphi < \frac{180}{c}\cdot i \quad \wedge \quad \frac{180}{c}\cdot(j-1) \le \theta < \frac{180}{c}\cdot j \right\}.$$
6. Spherical histogram consists of a sphere, serving as a reference object, and up to c^2 cylinders, whose main axes of symmetry are parallel to vectors that are representatives of each class and whose heights equal appropriate $n_{i,j}$ values. Two first spherical coordinates of the class representatives should be calculated using the formula
$$\varphi = \frac{180}{c}\cdot\left(i-\frac{1}{2}\right), \theta = \frac{180}{c}\cdot\left(j-\frac{1}{2}\right). \tag{6}$$

Spherical histograms enable visual assessment of the typical fiber orientation in a beam. Histograms shown in Fig. 7(a) and Fig. 7(b) include fiber orientation of the whole beam, but through appropriate narrowing the data range the orientation of fibers in different parts of the beam can be analyzed and compared with each other.

Since the fiber orientation in the beam is one of the most important parameters that determine the beam strength, angle values θ_k should be studied, as that are the angles between the beam main axis and a particular *k*-th fiber.

First, the mean $\bar{x}$ and the standard deviation σ should be calculated. Relying on the three sigma rule it can be considered, that the inclination angle of approximately 2/3 of the fibers from the beam main axis will be between $\bar{x} - \sigma$ and $\bar{x} + \sigma$.

Using the Pearson's chi-squared test a distribution can be fitted to the two dimensional histogram of angles θ. The null hypothesis states that the analyzed parameter has a particular distribution, whereas the alternative hypothesis claims the opposite. The higher the value of the parameter *p*, the better the distribution fits the analyzed data, since *p* denotes the probability of a type I error (the propability that rejecting the null hypothesis would be incorrect) [13].

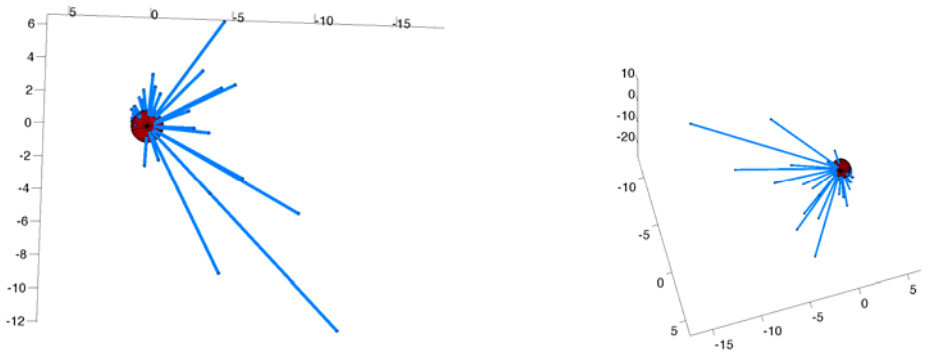

(a)

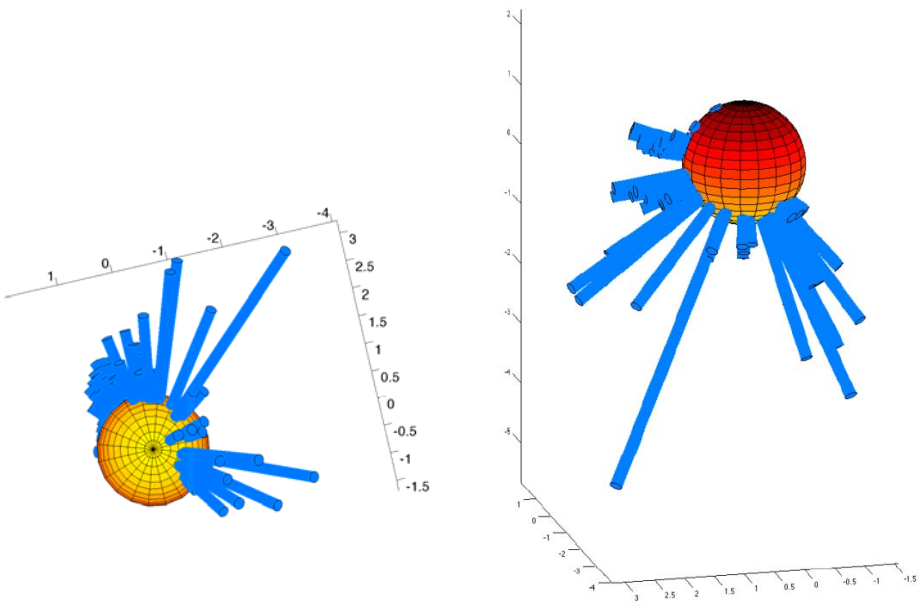

(b)

Fig. 7: Exemplary spherical histograms for (a) c = 10 (2 views), (b) c = 30 (2 views)

5 EXPERIMENTAL RESULTS AND DISCUSSION

Five distributions were fitted to the histograms of θ (Fig. 8(a)-3(e)) [18]:

- normal,
- exponential,
- gamma,
- lognormal,
- chi-squared.

A good fit was obtained for the gamma distribution (Fig. 8(c)), however, the best fitted distribution is the exponential one (Fig. 8(b)).

Another useful statistical tool is the Welch's t-test, which is an adaptation of Student's t-test intended for use with two samples having possibly unequal variances. It can be used to verify the

hypothesis, that the fiber orientation does not depend on their position in the beam (upper/lower part or beam end/center).

The null hypothesis states that the mean angles θ are equal for various beam parts and the alternative hypothesis is that they are different.

Our preliminary examinations resulted in the conclusion that fibers in the upper part of the beam have a greater tendency to form parallel to the beam axis and those in the lower part are characterized by a larger orientation variety. On the other hand according to the test results, the average angle θ does not depend on the beam part in terms of its end or center.

Due to the exponential nature of the angle between the fibers and the axis of the beam, the hypothesis that this angle is nearly 0, might be tested using a one-sample t-test. The preliminary studies showed that this angle is significantly different from zero. Therefore it cannot be assumed that the fibers are arranged parallel to the axis of the beam, although the observation of the 3D graphs and further analysis showed that they have this tendency. Thus it should be concluded that the arrangement of fibers in 3D space creates an object that resembles more a cone than a cylinder.

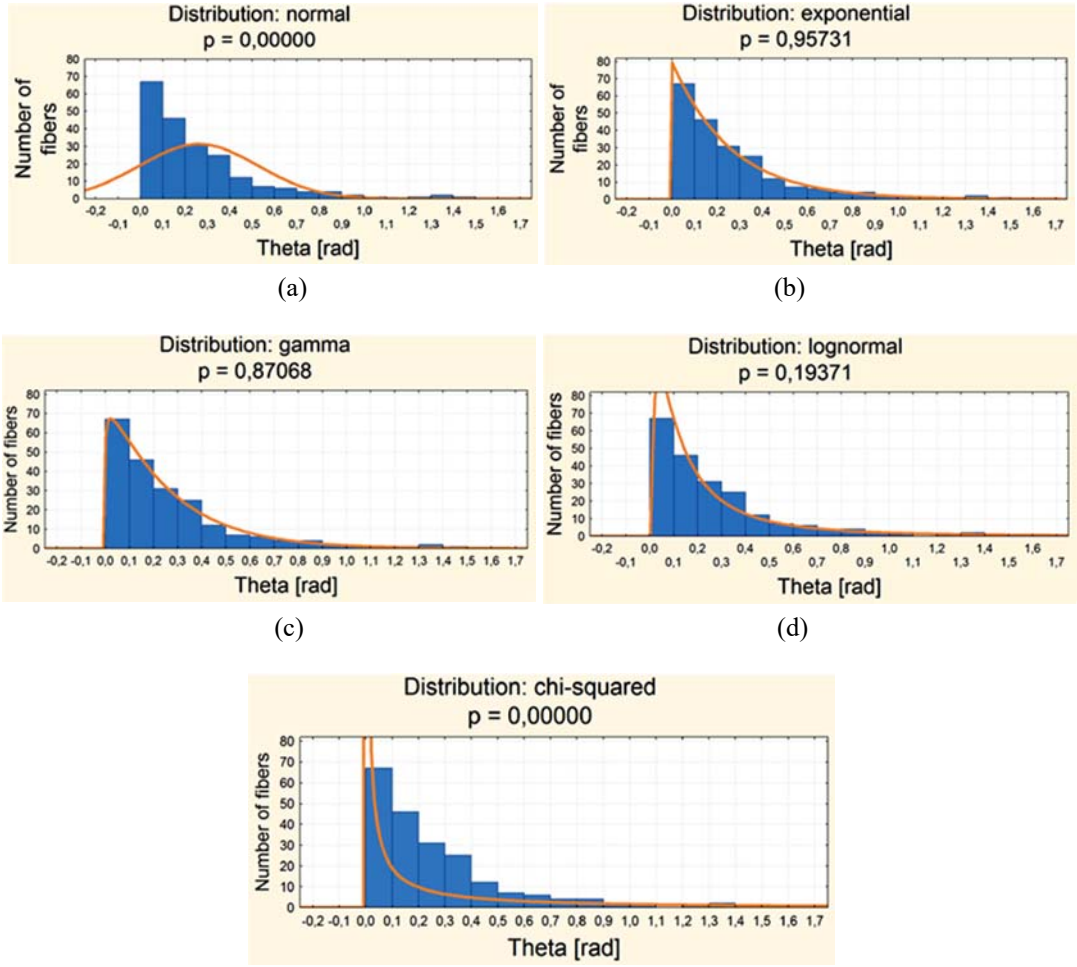

Fig. 8: Tested distributions: (a) normal, (b) exponential, (c) gamma, (d) log-normal, (e) chi [18]

The results, presented below are based on investigation of the whole concrete element (Fig. 9), consisting of 9 sections. The full report generated by the computer program is very large, so only a

local analysis of 1 micro-section is presented here. Fig. 9 shows a pictorial presentation of the results of a fibre count in a selected cross-section of concrete C2 divided into 16 x 16 squares. On this basis we determine the real distribution of fibres per unit of area in the sample cross-section.

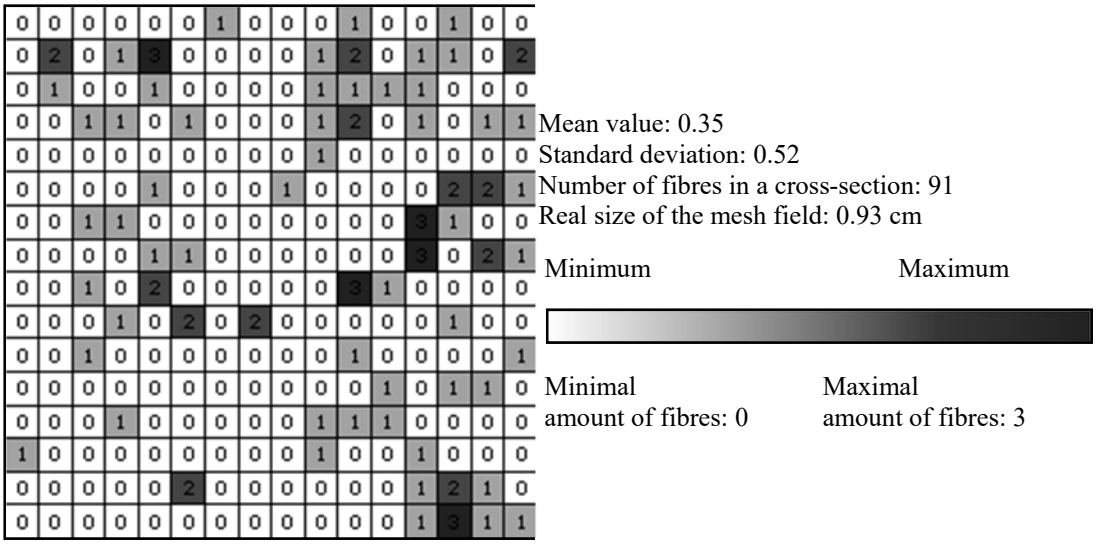

Fig. 9: Example of a concrete C2 cross-section for the division 16 x 16
and analysis of the number of fibres

Fig. 10 is a pictorial presentation of the results of the fibre count in a selected cross-section of concrete C2 with a division mesh 1 x 16 (rows). On this basis we can determine the summary distribution of fibres in horizontal cross-sections of the concrete sample, describing their local and global 3-dimensional concentration in a horizontal direction.

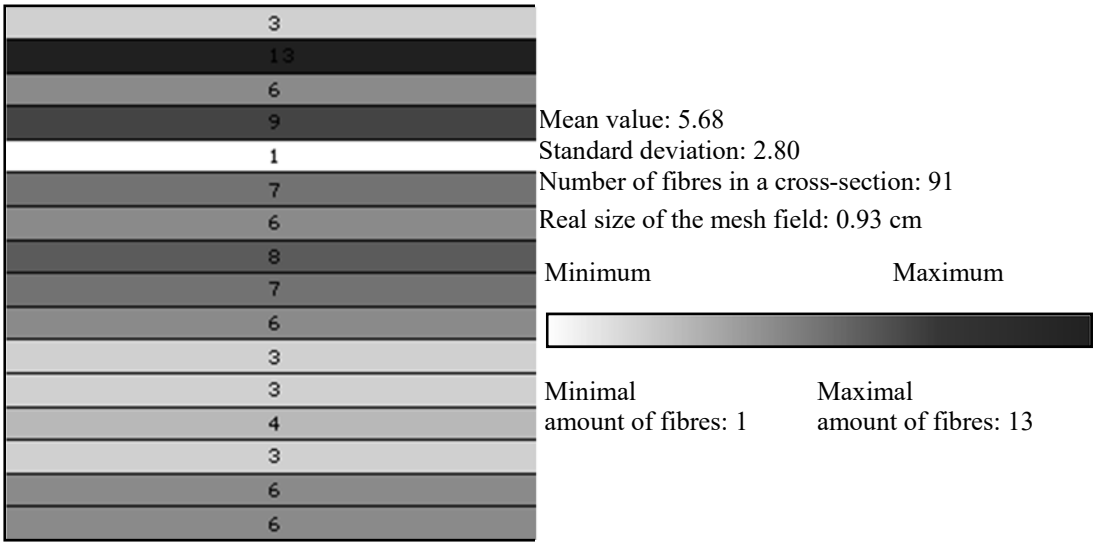

Fig. 10: Example of a concrete C2 cross-section for the division 16 x 16
and analysis of the number of fibres, data from the rows

Fig. 11 is the pictorial presentation of the results of the fibre count in a selected cross-section of concrete C2 with a division mesh 1 x 16 (columns). On this basis we can determine the summary

distribution of fibres in vertical cross-sections of the concrete sample, describing their local and global 3-dimensional concentration in a vertical direction.

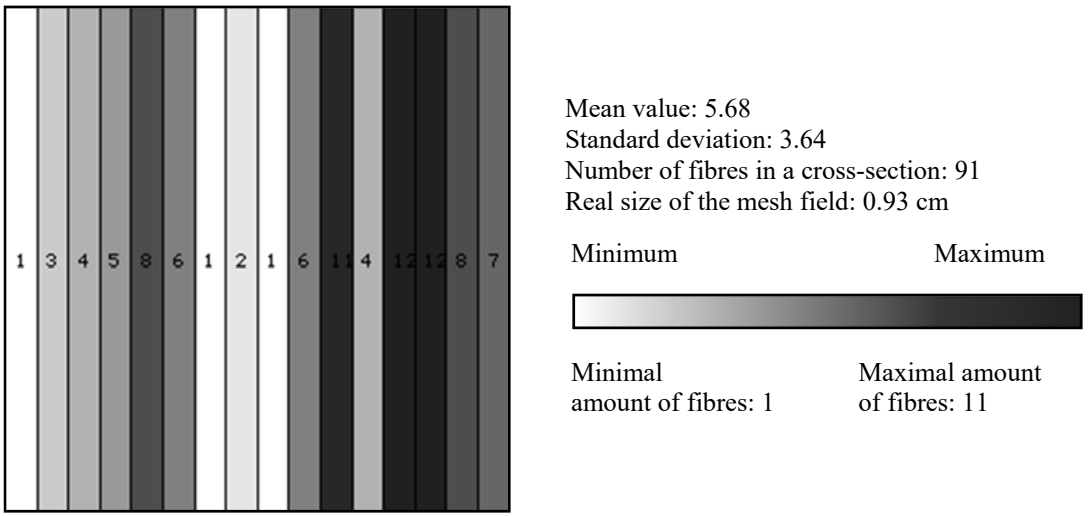

Fig. 11: Example of a concrete C2 cross-section for the division 16 x 16 and analysis of the number of fibres, data from the columns

The application of global scale to a substantial extent decreases the transparency of result presentation, because depending on the degree of divisions, the number of fibres in a sampled field fluctuated from 0 to 53. The global results are obtained by generating diagrams illustrating the number of fibres in cross-sections and in the whole concrete structural element. Figures 12-14 show the results for the selected three of nine sections of the test element made of C3 fibre concrete, mesh 32 x 32. On the basis of deployment of fibres in a sample, one can tell what the general trends of their dispersion are.

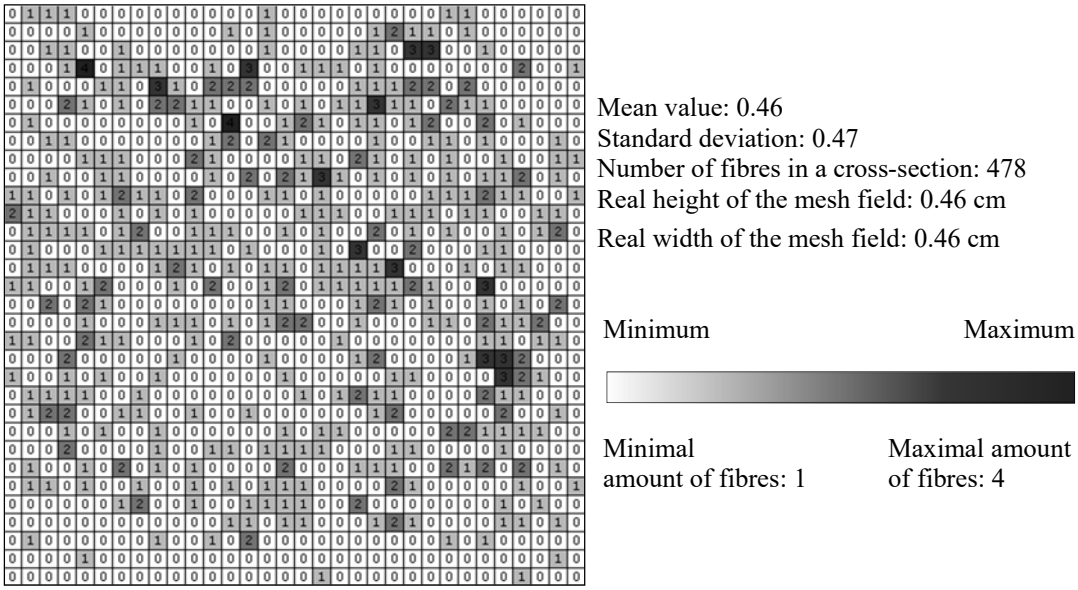

Fig. 12: Cross-section 200 mm of concrete C3 for the division 32 x 32 and analysis of the number of fibres

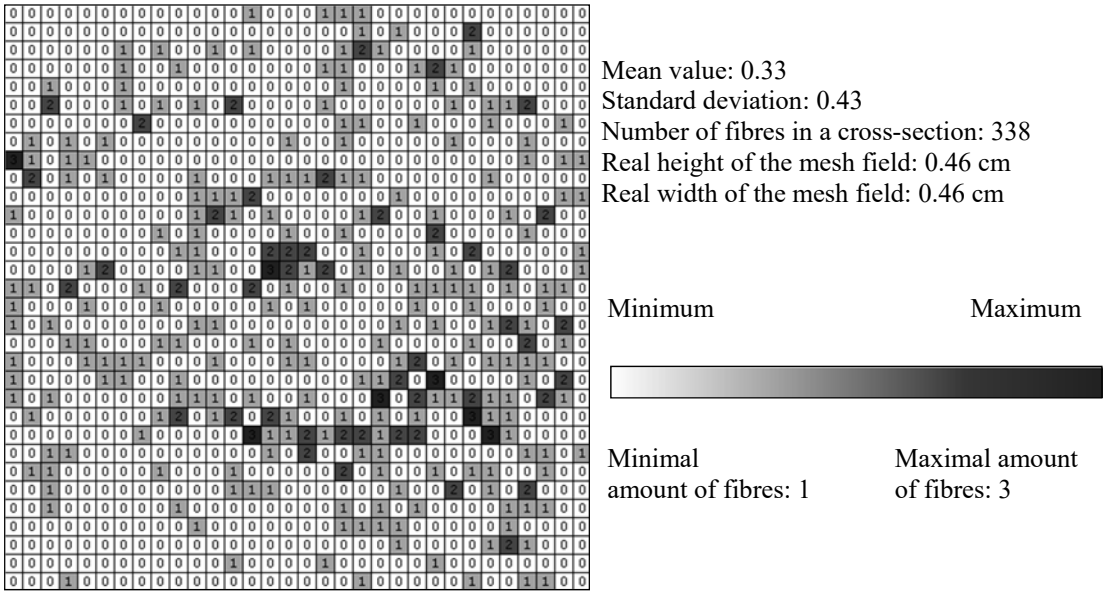

Fig. 13: Cross-section 400 mm of concrete C3 for the division 32 x 32 and analysis of the number of fibres

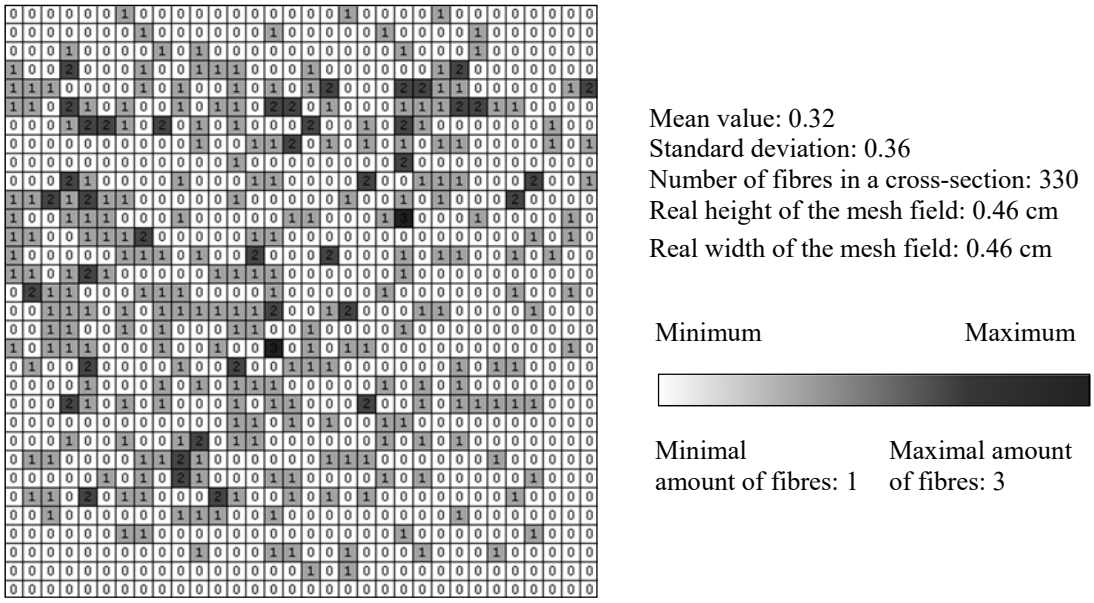

Fig. 14: Cross-section 500 mm of concrete C3 for the division 32 x 32 and analysis of the number of fibres

The results of the computer tomography studies are presented in Figures 15 - 18. 2D sections of concrete beams for the sections of C4: 100 mm, 200 mm, 400 mm and 550 mm from the edge of the concrete are shown in Figures 12. It should be noted that the characteristic rounding of edges of individual sections of images result from the scanning method, not from the internal structure of the concrete. The selected sections of the concrete in question prove generally to have an even distribution of fibres in the volume of the test concrete. There are no large clumps of fibres in a

matrix of concrete. Visually it could be considered a parallel arrangement of fibers to the direction of flow of the addition to the mixture in the process of formation. There are only a few fibres arranged perpendicularly to the direction of formation.

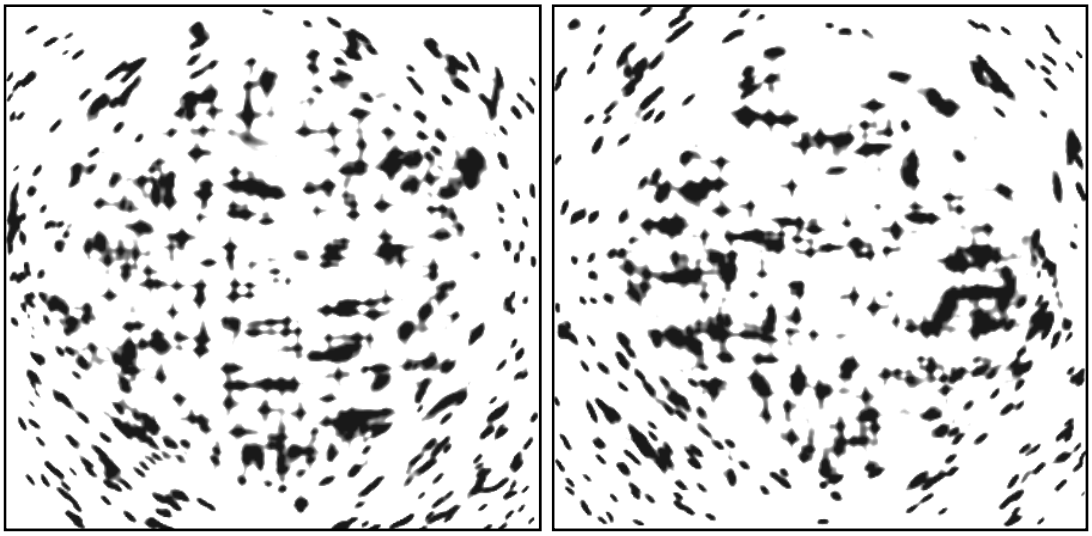

Fig. 15: 2D sections of concrete beams for the sections of C4:
100 mm, 200 mm from the edge of concrete

Rheological parameters and X-ray 2D sections of SFRHPSCC beams for different kind of fibres and volume are presented in Figures 16.

In general, increasing fibre content causes linear increase of yield value *g* of SFRHPSCC. Nature and range of influence of fibres content on plastic viscosity *h* of SFRHPSCC also depends on the matrix properties and on the fibre length. A 3D cross-section of the concrete beam section C2 for 400-500 mm from the edge of the concrete is shown in Figures 17 and 18. 3D image confirms the trend of the directional orientation of fibers in a matrix of concrete. The fibres are generally evenly distributed in concrete, with the exception of selected sections of the edge of the concrete.On the basis of computed tomography, uneven distribution of steel fibres in concrete volume samples was proved. Whereas, no high concentrations of fibres in concrete matrix were detected. Also, the parallel distribution of fibres was confirmed, in accordance with the direction of movement of the mixture during casting, especially in the case of SW35 fibres. Only few fibres were perpendicularly oriented to this direction. The radial arrangement of fibres in the vicinity of the corners of bars cross-section is associated with the slower movement of the mixture close to the mould walls. This is due to higher frictional resistance occurring in those areas. The tests have shown that computed tomography gives the possibility of the distribution of steel fibres in the entire volume of concrete examination, and also in small, selected areas. Such analysis allows to obtain two-dimensional (2D) and three dimensional (3D) images of fibres distribution. Obtained results may present the basis for the development of designing methods of self-compacting fibres reinforced concrete, including the form of structural elements. The key problem is to determine changes in distribution of dispersed reinforcement in various structures, depending on used technology of mixture casting and its rheological properties, and also the volume and geometrical forms of steel fibres. Obtained results may also be used for modelling of the properties of selected structural elements.

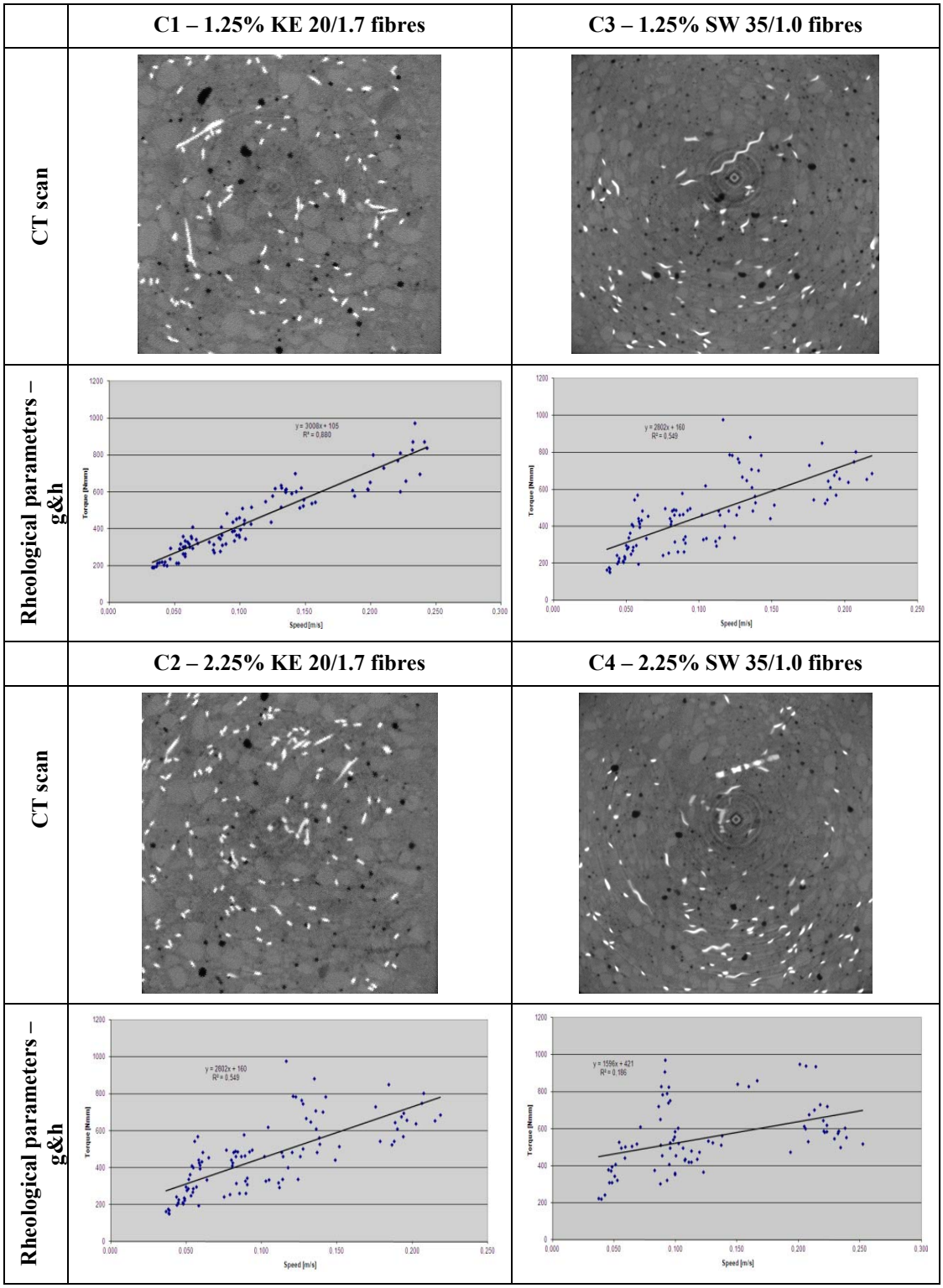

Fig. 16: Rheological parameters and X-ray 2D sections of SFRHPSCC beams for different kind of fibres and volume

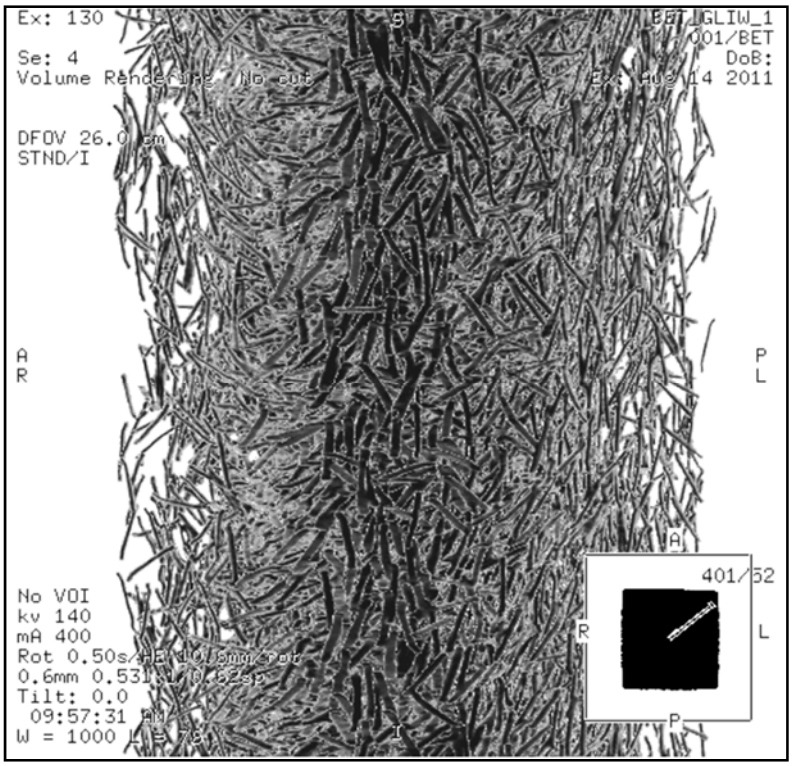

Fig. 17: X-ray 3D sections of concrete beams C2 for the sections of 400 ÷ 500 mm from the edge of concrete

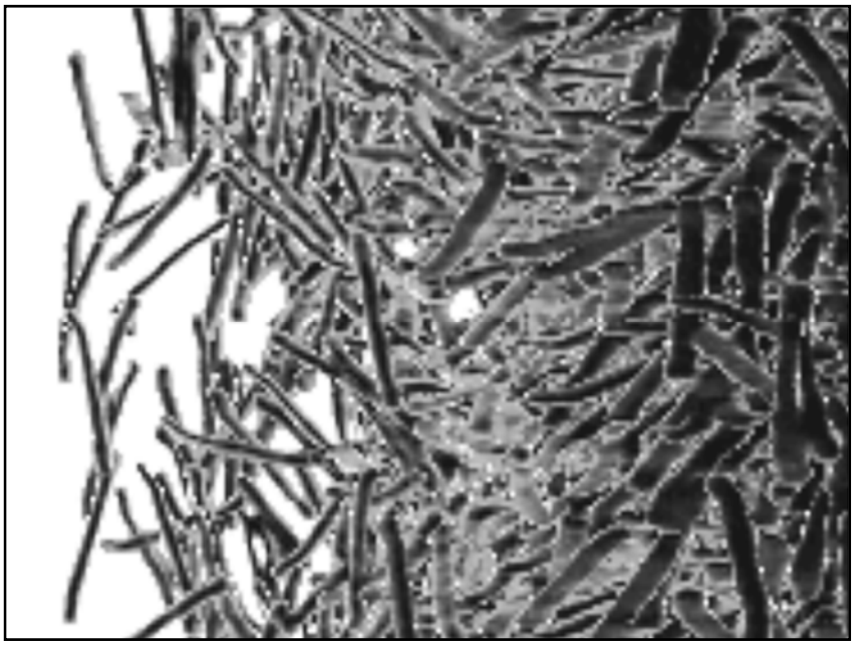

Fig. 18: X-ray 3D area sections of concrete beams C2 for the sections of 450 mm from the edge of concrete

6 CONCLUSIONS

On the basis of our own studies, using our own method and software to analyze the distribution of fibres in concrete, as well as the tomography examinations, the results were obtained within the selected field of research.

The developed computer program allows the analysis of the distribution of individual fibres in samples, both in the global and local systems. It also allows the identification of trends in the distribution of fibres, depending on the direction of concrete mix formation, proximity of the walls of molds and up - down orientation of the form. The computed tomography shows the inner space of concrete with steel fibers in 2D and 3D formats without any limitations.

Both of the applied methods of identifying the deployment of fibre in the concrete SFRHPSCC fibres revealed no tendency for the fibres to stick to the walls of the form, no effects of the wall. It has been observed that there were fewer steel fibres in the immediate proximity of the form walls.

An image analysis method for automatic segmentation and evaluation of steel fibers was presented. For qualitative assessment of typical fibers orientation a 4D histogram was proposed. Preliminary quantitative analysis showed that the fibers orientation along the beam exhibit an exponential distribution.

Generic statistical models that combine the method of forming, fibers and pores position and orientation with mechanical beam properties are the main subject of future research. As a preliminary step the image processing software allowing automatic fibers and air pores segmentation providing data on position, orientation and shape properties has to be developed.

The number of fibers positioned in most cases parallel to the longitudinal walls of the form leads to the conclusion that such behavior results from the direction of concrete dispersing in the form. The presented method and software is the introduction to research on the relationship between the distribution of fibers in concrete elements and the strength parameters.

Confirmed was the orientation of fibres consistent with the direction of the formation of a mixture SFRHPSCC. Proved as well was the uniform distribution of fibers in the tested concrete. There was no evidence of fibers too closely placed to each other and the formation of so-called "hedgehogs".

REFERENCES

[1] DING, Y., THOMASETH, D., NIEDEREGGER, CH., THOMAS, A., LUKAS, W. The investigation on the workability and flexural toughness of fibre cocktail reinforced self-compacting high performance concrete, in: 6th RILEM Symposium on fibre-reinforced concretes (FRC) – BEFIB 2004, Varenna, Italy 2004.

[2] SIRIJAROONCHAI, K., EL-TAWIL, S., PARRA-MONTESINOS, G. *Behavior of high performance fiber reinforced cement composites under multi-axial compressive loading*, Cement & Concrete Composites, article in press, 2009.

[3] DING, Y., AZEVEDO, C., AGUIAR, J.B., JALALI, S. Study on residual behaviour and flexural toughness of fibre cocktail reinforced self-compacting high performance concrete after exposure to high temperature, Construction and Building Materials 26 (2012) pp. 21–31.

[4] DING, Y., LIU, S., ZHANG, Y., THOMAS, A. The investigation on the workability of fibre cocktail reinforced self-compacting high performance concrete, Construction and Building Materials, 2008, 22, pp. 1462–1470.

[5] KANG, S.-T., KIM, J.-K. Investigation on the flexural behavior of UHPCC considering the effect of fiber orientation distribution, Construction and Building Materials, 2011, 28, pp. 57–65.

[6] KANG, S.-T., KIM, J.-K. The relation between fiber orientation and tensile behavior in an Ultra High Performance Fiber Reinforced Cementitious Composites (UHPFRCC), Cement and Concrete Research, 2011, 41, pp. 1001–1014.

[7] TANIKELLA, P.N.D., GETTU, R. *On the distribution of fibers in self-compacting concrete*. 7th RILEM Symposium on Fibre - Reinforced Concretes (FRC) - BEFIB 2008, Chennai, India, pp. 1147-1153.

[8] TORRIJOS, M.C., TOBES, J.M., BARRAGÁN, B.E., ZERBINO, R.L. *Orientation and distribution of steel fibres in self-compacting concrete.* 7th RILEM Symposium on Fibre - Reinforced Concretes (FRC) - BEFIB 2008, Chennai, India, pp. 729 - 738.

[9] VANDEWALLE, L., HEIRMAN, G., VAN RICKSTAL, F. *Fibre orientation in self-compacting fibre reinforced concrete*. 7th RILEM Symposium on Fibre - Reinforced Concretes (FRC) - BEFIB 2008, Chennai, India, pp. 719 - 728.

[10] YARDIMCI, M.Y., BARADAN, B., TAŞDEMIR, M.A. *Studies on the relation between fiber orientation and flexural performance of SFRSCC*. 7th RILEM Symposium on Fibre - Reinforced Concretes (FRC) - BEFIB 2008, Chennai, India, pp. 711-718.

[11] STROEVEN, P. AND SHAH P., S.P. *Use of radiography-image analysis for steel fibre reinforced concrete*. In. "Testing and Test Methods of Fibre Reinforced Composites", R.N. Swamy ed. Construction Press, Lancaster, 1978, pp. 308-311.

[12] TATTARSALL, G H, BANFILL, P.F.G. 1983. *The Rheology of Fresh Concrete.* Boston: Pitman Books Limited. 356 p.

[13] PONIKIEWSKI, T., GOŁASZEWSKI, J. The new approach to the study of random distribution of fibres in high performance self-compacting concrete, Cement Wapno Beton, 2012, 79, pp. 165 - 176.

[14] BRANDT, A.M. Cement-based composites. Materials, mechanical properties and performance, Taylor & Francis, USA & Canada 2009.

[15] PONIKIEWSKI, T., CYGAN, G. Some properties of self-compacting concretes reinforced with steel fibres, Cement Wapno Beton, 2011, 78, pp. 203-209.

[16] PAJĄK M., PONIKIEWSKI, T. Flexural behavior of self-compacting concrete reinforced with different types of steel fibers, Construction and Building Materials, 2013, 47, pp. 397–408.

[17] IBÁÑEZ L., SCHROEDER W., NG L., CATES J. *The ITK Software Guide*. Kitware, 2005. available: http://www.itk.org/ItkSoftwareGuide.pdf

[18] RUDZKI, M., BUGDOL, M., PONIKIEWSKI, T. Determination of steel fibers orientation in SCC using computed tomography and digital image analysis methods, Cement Wapno Beton, 2013, R.18, 5, pp. 257-263.

[19] PONIKIEWSKI, T., GOŁASZEWSKI, J., BUGDOL, M., RUDZKI, M. *Determination of steel fibres distribution in self-compacting concrete beams using X-ray computed tomography*, Archives of Civil and Mechanical Engineering, 2014, 15, pp. 558-568.

Reviewers:

Prof. Ing. Leonard Hobst, CSc., Institute of Building Testing, Faculty of Civil Engineering, Brno University of Technology, Czech Republic.

Ing. Vlastimil Bílek, Ph.D., Department of Building Materials and Diagnostics of Structures, Faculty of Civil Engineering, VŠB – Technical University of Ostrava, Czech Republic.